Supplementary Material

Face-Sharing Heterotrinuclear M^{II}–Ln^{III}–M^{II} (M = Mn, Fe, Co, Zn; Ln = La, Gd, Tb, Dy) Complexes: Synthesis, Structures, Magnetic and SMM Properties

Tomoka Yamaguchi,[a] Jean-Pierre Costes,[b]* Yukana Kishima,[a] Masaaki Kojima,[a]* Yukinari Sunatsuki,[a] Nicolas Bréfuel,[b] Jean-Pierre Tuchagues,[b] Laure Vendier,[b] Wolfgang Wernsdorfer[c]

[a] *Department of Chemistry, Faculty of Science, Okayama University, Tsushima-naka 3-1-1, Okayama 700-8530*

[b] *Laboratoire de Chimie de Coordination du CNRS, UPR 8241, liée par conventions à l'Université Paul Sabatier et à l'Institut National Polytechnique de Toulouse, 205 route de Narbonne, 31077 Toulouse Cedex (France)*

Fax : 33 (0)5 61 55 30 03, e-mail : costes@lcc-toulouse.fr

[c] *Laboratoire Louis Néel du CNRS, BP 166, 38042 GRENOBLE Cedex 9, France*

Table S1. Selected bond lengths, distances and angles for complexes **1**, **2** and **3**.

	CoGdCo **1**	CoTbCo **2**	CoDyCo **3**		**1** sym	**2** sym
Co(1)-N(1)	2.087(6)	2.095(3)	2.093(5)	Co(3)-N(7)	2.094(7)	2.099(4)
Co(1)-N(2)	2.107(7)	2.119(3)	2.106(5)	Co(3)-N(8)	2.105(7)	2.097(4)
Co(1)-N(3)	2.125(7)	2.108(3)	2.119(5)	Co(3)-N(9)	2.102(7)	2.077(4)
Co(1)-O(1)	2.080(5)	2.086(3)	2.098(4)	Co(3)-O(13)	2.056(5)	2.062(3)
Co(1)-O(2)	2.085(5)	2.078(2)	2.130(3)	Co(3)-O(15)	2.064(5)	2.062(3)
Co(1)-O(3)	2.076(5)	2.078(3)	2.086(4)	Co(3)-O(16)	2.059(5)	2.073(3)
Co(2)-N(4)	2.088(7)	2.114(4)	2.118(5)	Ln(2)-O(13)	2.416(5)	2.427(3)
Co(2)-N(5)	2.089(7)	2.098(4)	2.123(5)	Ln(2)-O(14)	2.955(5)	2.963(3)
Co(2)-N(6)	2.093(7)	2.101(3)	2.120(5)	Ln(2)-O(15)	2.440(5)	2.383(3)
Co(2)-O(4)	2.076(5)	2.061(3)	2.101(4)	Ln(2)-O(16)	2.450(5)	2.407(3)
Co(2)-O(5)	2.077(5)	2.086(3)	2.099(4)	Ln(2)-O(17)	2.869(5)	2.900(3)
Co(2)-O(6)	2.057(6)	2.092(3)	2.115(4)	Ln(2)-O(18)	2.980(5)	2.985(3)
Ln(1)-O(1)	2.417(5)	2.382(3)	2.386(3)	Co(3)-Ln(2)	3.3312(13)	3.3064(6)
Ln(1)-O(2)	2.397(5)	2.380(3)	2.382(4)	Co(3)-O(13)-Ln(2)	96.0(2)	94.52(11)
Ln(1)-O(3)	2.456(5)	2.403(3)	2.385(4)	Co(3)-O(15)-Ln(2)	95.0(2)	95.85(10)
Ln(1)-O(4)	2.402(5)	2.403(3)	2.395(4)	Co(3)-O(16)-Ln(2)	94.84(18)	94.82(10)
Ln(1)-O(5)	2.409(6)	2.380(3)	2.367(3)	O(13)-Co(3)-O(15)	77.8(2)	78.65(11)
Ln(1)-O(6)	2.429(5)	2.408(3)	2.360(3)	O(13)-Co(3)-O(16)	78.8(2)	77.29(11)
Ln(1)-O(7)	2.897(5)	2.937(3)	2.912(4)	O(15)-Co(3)-O(16)	77.8(2)	77.33(11)
Ln(1)-O(8)	2.893(5)	2.909(3)	2.957(8)	O(13)-Ln(2)-O(15)	64.41(17)	65.79(9)
Ln(1)-O(9)	2.912(5)	2.912(3)	2.864(4)	O(13)-Ln(2)-O(16)	64.94(18)	64.56(9)
Ln(1)-O(10)	2.934(5)	2.908(3)	2.931(4)	O(15)-Ln(2)-O(16)	63.94(17)	65.26(9)
Ln(1)-O(11)	2.983(5)	2.913(3)	2.868(4)	Co(3)-Ln(2)-Co(3)	178.68(5)	178.42(2)
Ln(1)-O(12)	2.896(5)	2.995(3)	2.899(4)			
Co(1)-Ln(1)	3.3214(13)	3.3027(5)	3.3034(8)			
Co(2)-Ln(1)	3.3128(13)	3.3024(6)	3.3007(8)			
Co(1)-O(1)-Ln(1)	94.9(2)	95.09(10)	94.68(14)			
Co(1)-O(2)-Ln(1)	95.4(2)	95.37(10)	93.98(14)			
Co(1)-O(3)-Ln(1)	93.9(2)	94.67(10)	95.04(14)			
Co(2)-O(4)-Ln(1)	95.2(2)	95.12(10)	94.22(13)			
Co(2)-O(5)-Ln(1)	94.9(2)	95.15(10)	95.10(14)			
Co(2)-O(6)-Ln(1)	94.9(2)	94.18(10)	94.87(13)			
O(1)-Co(1)-O(2)	76.7(2)	76.48(10)	77.01(14)			
O(1)-Co(1)-O(3)	78.9(2)	77.69(10)	76.88(14)			
O(2)-Co(1)-O(3)	78.57(19)	77.43(10)	77.33(15)			
O(4)-Co(2)-O(5)	77.4(2)	76.75(11)	76.59(14)			
O(4)-Co(2)-O(6)	77.3(2)	78.80(11)	77.43(14)			
O(5)-Co(2)-O(6)	78.9(2)	77.13(10)	76.25(14)			
O(1)-Ln(1)-O(2)	64.95(17)	65.54(9)	67.02(12)			
O(1)-Ln(1)-O(3)	65.60(16)	66.15(8)	66.08(13)			
O(2)-Ln(1)-O(3)	65.75(16)	65.83(9)	67.11(12)			
O(4)-Ln(1)-O(5)	65.36(17)	65.12(9)	66.26(12)			
O(4)-Ln(1)-O(6)	64.61(18)	66.45(9)	67.36(13)			
O(5)-Ln(1)-O(6)	65.77(17)	65.90(9)	66.78(13)			
Co(1)-Ln(1)-Co(2)	178.41(5)	177.864(15)	176.93(2)			

Table S2. Selected bond lengths, distances and angles for complexes **5**, **6** and **7**.

	MnGdMn **5**	MnTbMn **6**	MnDyMn **7**
Mn(1)-N(1)	2.184(4)	2.192(5)	2.184(4)
Mn(1)-N(2)	2.187(4)	2.191(5)	2.205(4)
Mn(1)-N(3)	2.204(4)	2.207(4)	2.187(4)
Mn(1)-O(1)	2.172(3)	2.142(4)	2.169(3)
Mn(1)-O(2)	2.138(3)	2.168(4)	2.140(3)
Mn(1)-O(3)	2.128(3)	2.130(4)	2.144(3)
Mn(2)-N(4)	2.202(4)	2.202(5)	2.188(4)
Mn(2)-N(5)	2.194(4)	2.193(5)	2.206(4)
Mn(2)-N(6)	2.189(4)	2.204(5)	2.183(4)
Mn(2)-O(4)	2.165(3)	2.143(4)	2.174(3)
Mn(2)-O(5)	2.146(3)	2.166(4)	2.146(3)
Mn(2)-O(6)	2.143(3)	2.149(4)	2.142(3)
Ln(1)-O(1)	2.420(3)	2.377(3)	2.392(3)
Ln(1)-O(2)	2.406(3)	2.388(4)	2.389(3)
Ln(1)-O(3)	2.418(3)	2.385(3)	2.383(3)
Ln(1)-O(4)	2.400(3)	2.392(4)	2.373(3)
Ln(1)-O(5)	2.401(3)	2.371(3)	2.371(3)
Ln(1)-O(6)	2.434(3)	2.371(3)	2.397(3)
Ln(1)-O(7)	2.924(3)	2.946(4)	2.937(4)
Ln(1)-O(8)	2.895(3)	2.990(4)	2.884(3)
Ln(1)-O(9)	2.916(3)	2.891(4)	2.991(4)
Ln(1)-O(10)	2.885(3)	2.901(4)	2.923(4)
Ln(1)-O(11)	2.956(3)	2.976(4)	2.896(3)
Ln(1)-O(12)	2.971(3)	2.929(4)	2.968(4)
Mn(1)-Ln(1)	3.3339(7)	3.3226(9)	3.3067(6)
Mn(2)-Ln(1)	3.3355(7)	3.3257(9)	3.3074(6)
Mn(1)-O(1)-Ln(1)	92.91(11)	94.51(13)	92.81(10)
Mn(1)-O(2)-Ln(1)	94.21(11)	93.53(14)	93.63(11)
Mn(1)-O(3)-Ln(1)	94.12(11)	94.60(13)	93.68(11)
Mn(2)-O(4)-Ln(1)	93.75(10)	94.19(13)	93.22(10)
Mn(2)-O(5)-Ln(1)	94.19(11)	94.17(13)	94.02(11)
Mn(2)-O(6)-Ln(1)	93.33(11)	94.61(14)	93.39(10)
O(1)-Mn(1)-O(2)	77.79(11)	76.94(14)	77.80(11)
O(1)-Mn(1)-O(3)	77.94(11)	75.87(14)	77.57(11)
O(2)-Mn(1)-O(3)	76.73(12)	76.85(14)	76.42(11)
O(4)-Mn(2)-O(5)	76.98(11)	77.11(14)	77.84(11)
O(4)-Mn(2)-O(6)	78.29(11)	75.62(14)	76.23(11)
O(5)-Mn(2)-O(6)	76.74(11)	76.04(14)	77.80(11)
O(1)-Ln(1)-O(2)	68.21(10)	68.49(12)	68.94(10)
O(1)-Ln(1)-O(3)	67.98(10)	66.96(13)	68.93(9)
O(2)-Ln(1)-O(3)	66.58(10)	68.08(13)	67.46(10)
O(4)-Ln(1)-O(5)	67.95(10)	68.66(13)	68.84(10)
O(4)-Ln(1)-O(6)	68.46(10)	67.06(13)	69.27(10)
O(5)-Ln(1)-O(6)	66.83(10)	68.18(13)	67.44(10)
Mn(1)-Ln(1)-Mn(2)	177.886(19)	177.73(2)	177.551(18)

Table S3. Selected bond lengths, distances and angles for complexes **8**, **9** and **10**.

	FeGdFe **8**	FeTbFe **9**	FeDyFe **10**
Fe(1)-N(1)	2.145(5)	2.144(6)	2.137(5)
Fe(1)-N(2)	2.149(4)	2.145(8)	2.153(6)
Fe(1)-N(3)	2.159(5)	2.163(7)	2.146(5)
Fe(1)-O(1)	2.102(3)	2.101(5)	2.121(4)
Fe(1)-O(2)	2.092(3)	2.104(5)	2.096(4)
Fe(1)-O(3)	2.112(3)	2.097(5)	2.111(4)
Fe(2)-N(4)	2.148(5)	2.157(7)	2.146(5)
Fe(2)-N(5)	2.139(4)	2.140(7)	2.142(5)
Fe(2)-N(6)	2.166(4)	2.155(6)	2.164(5)
Fe(2)-O(4)	2.110(3)	2.119(5)	2.111(4)
Fe(2)-O(5)	2.114(3)	2.113(5)	2.087(4)
Fe(2)-O(6)	2.100(3)	2.096(5)	2.123(4)
Ln(1)-O(1)	2.382(3)	2.376(4)	2.370(4)
Ln(1)-O(2)	2.402(3)	2.382(5)	2.395(4)
Ln(1)-O(3)	2.400(3)	2.408(5)	2.358(5)
Ln(1)-O(4)	2.382(3)	2.407(5)	2.365(4)
Ln(1)-O(5)	2.378(3)	2.387(5)	2.392(4)
Ln(1)-O(6)	2.402(3)	2.402(5)	2.379(4)
Ln(1)-O(7)	2.901(3)	2.957(5)	2.975(4)
Ln(1)-O(8)	2.886(3)	2.913(5)	2.897(4)
Ln(1)-O(9)	2.954(4)	2.878(5)	2.911(4)
Ln(1)-O(10)	2.933(4)	2.962(5)	2.914(4)
Ln(1)-O(11)	2.944(4)	2.901(5)	2.880(4)
Ln(1)-O(12)	2.889(3)	2.876(5)	3.002(4)
Fe(1)-Ln(1)	3.2960(9)	3.2741(12)	3.2656(9)
Fe(2)-Ln(1)	3.2905(9)	3.2801(12)	3.2665(9)
Fe(1)-O(1)-Ln(1)	94.42(12)	93.78(17)	93.13(14)
Fe(1)-O(2)-Ln(1)	94.09(11)	93.6(2)	93.04(15)
Fe(1)-O(3)-Ln(1)	93.64(12)	92.98(18)	93.72(15)
Fe(2)-O(4)-Ln(1)	94.01(12)	92.66(19)	93.56(15)
Fe(2)-O(5)-Ln(1)	93.99(11)	93.40(19)	93.42(15)
Fe(2)-O(6)-Ln(1)	93.70(12)	93.38(17)	92.84(15)
O(1)-Fe(1)-O(2)	76.87(13)	77.88(19)	79.23(16)
O(1)-Fe(1)-O(3)	78.10(12)	79.7(2)	77.89(16)
O(2)-Fe(1)-O(3)	78.28(13)	76.98(19)	76.56(16)
O(4)-Fe(2)-O(5)	77.54(13)	78.73(19)	76.71(16)
O(4)-Fe(2)-O(6)	76.59(13)	79.24(19)	78.61(15)
O(5)-Fe(2)-O(6)	78.74(13)	77.38(19)	78.79(16)
O(1)-Ln(1)-O(2)	66.05(11)	67.48(17)	68.70(14)
O(1)-Ln(1)-O(3)	67.44(10)	68.42(18)	68.48(14)
O(2)-Ln(1)-O(3)	67.09(10)	66.17(18)	66.50(14)
O(4)-Ln(1)-O(5)	67.53(11)	68.09(16)	66.39(14)
O(4)-Ln(1)-O(6)	66.10(12)	67.96(16)	68.83(13)
O(5)-Ln(1)-O(6)	68.00(11)	66.64(17)	68.12(13)
Fe(1)-Ln(1)-Fe(2)	178.19(19)	177.56(3)	176.93(2)

Table S4. Values of the symmetry measurements (octahedron and trigonal prism geometries) for the structurally characterized complexes.

		O_h (OC-6)	D_{3h} (TPR-6)
CoGdCo **1**	Co1(Gd1)	5.01	4.16
(*C*2/*c*)	Co2(Gd1)	5.02	4.17
	Co3(Gd2)	3.71	5.64
CoTbCo **2**	Co1(Tb1)	5.03	4.24
(*C*2/*c*)	Co2(Tb1)	5.03	4.20
	Co3(Tb2)	3.81	5.55
CoDyCo **3**	Co1(Dy)	6.98	2.65
($P2_12_12_1$)	Co2(Dy)	7.53	2.37
MnGdMn **5**	Mn1(Gd)	9.07	1.58
($P2_12_12_1$)	Mn2(Gd)	9.60	1.37
MnTbMn **6**	Mn1(Tb)	9.18	1.60
($P2_12_12_1$)	Mn2(Tb)	9.74	1.40
MnDyMn **7**	Mn1(Dy)	9.04	1.59
($P2_12_12_1$)	Mn2(Dy)	9.64	1.38
FeGdFe **8**	Fe1(Gd)	7.79	2.18
($P2_12_12_1$)	Fe2(Gd)	7.84	2.16
FeTbFe **9**	Fe1(Tb)	7.94	2.08
($P2_12_12_1$)	Fe2(Tb)	7.79	2.12
FeDyFe **10**	Fe1(Dy)	7.93	2.09
($P2_12_12_1$)	Fe2(Dy)	7.67	2.23

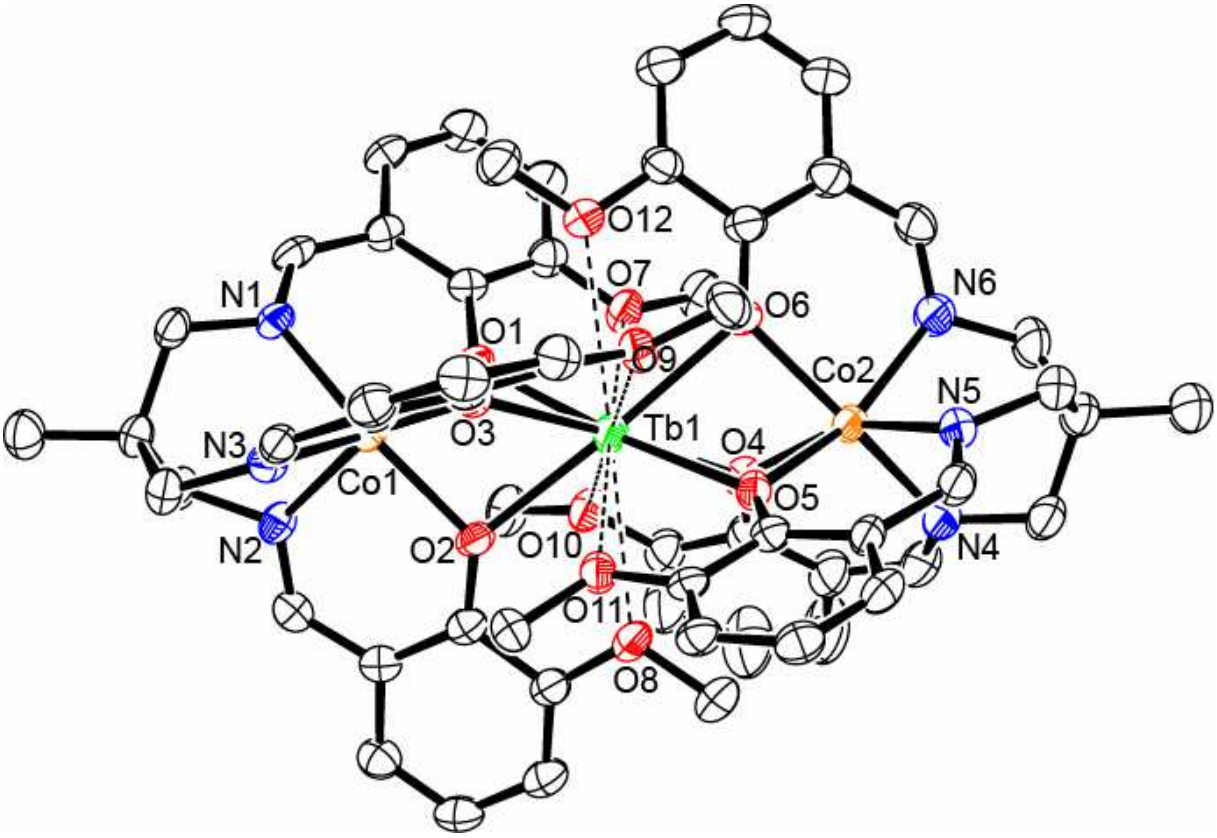

Figure S1. Molecular structure of the trinuclear $[LCoTbCoL]^{+}$ entity **2**, with the thermal ellipsoids drawn at the 30 % probability level. Hydrogen atoms are omitted for clarity.

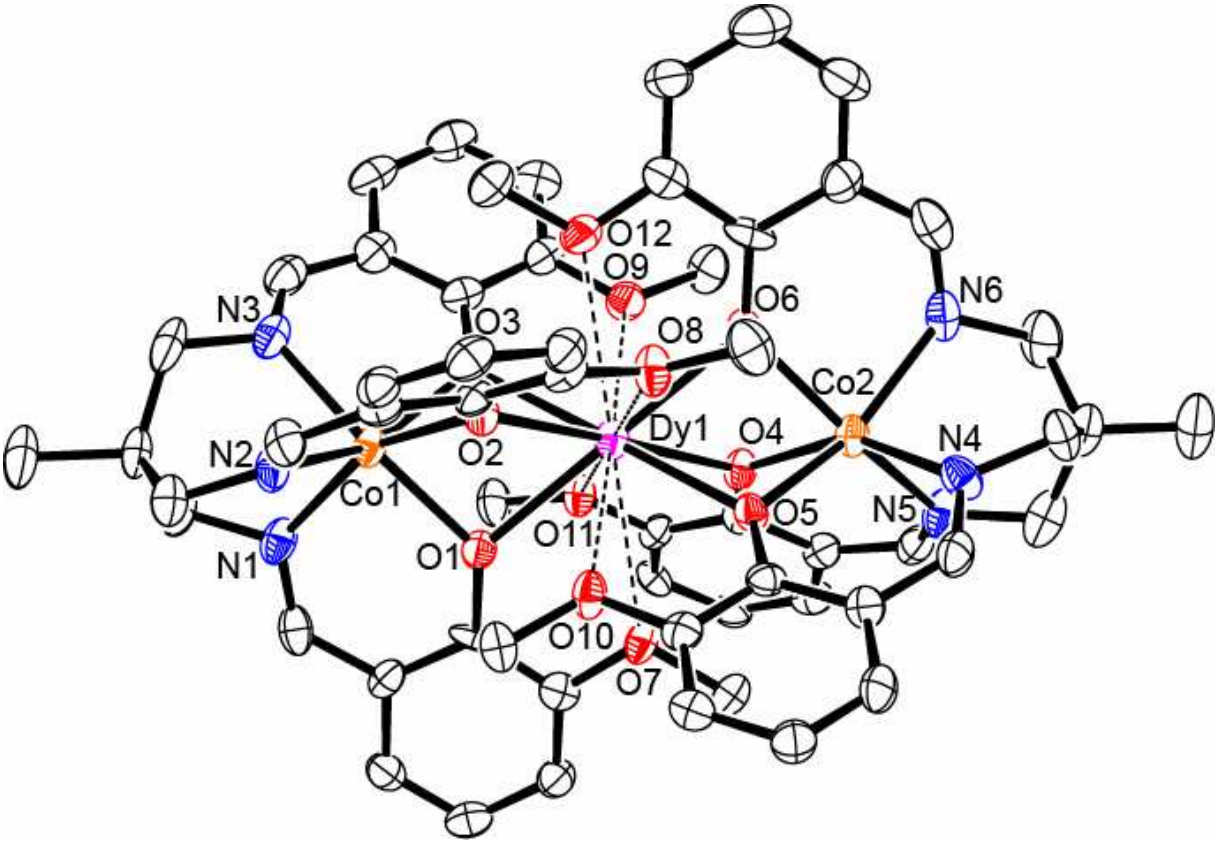

Figure S2. Molecular structure of the trinuclear $[LCoDyCoL]^{+}$ entity **3**, with the thermal ellipsoids drawn at the 30 % probability level. Hydrogen atoms are omitted for clarity.

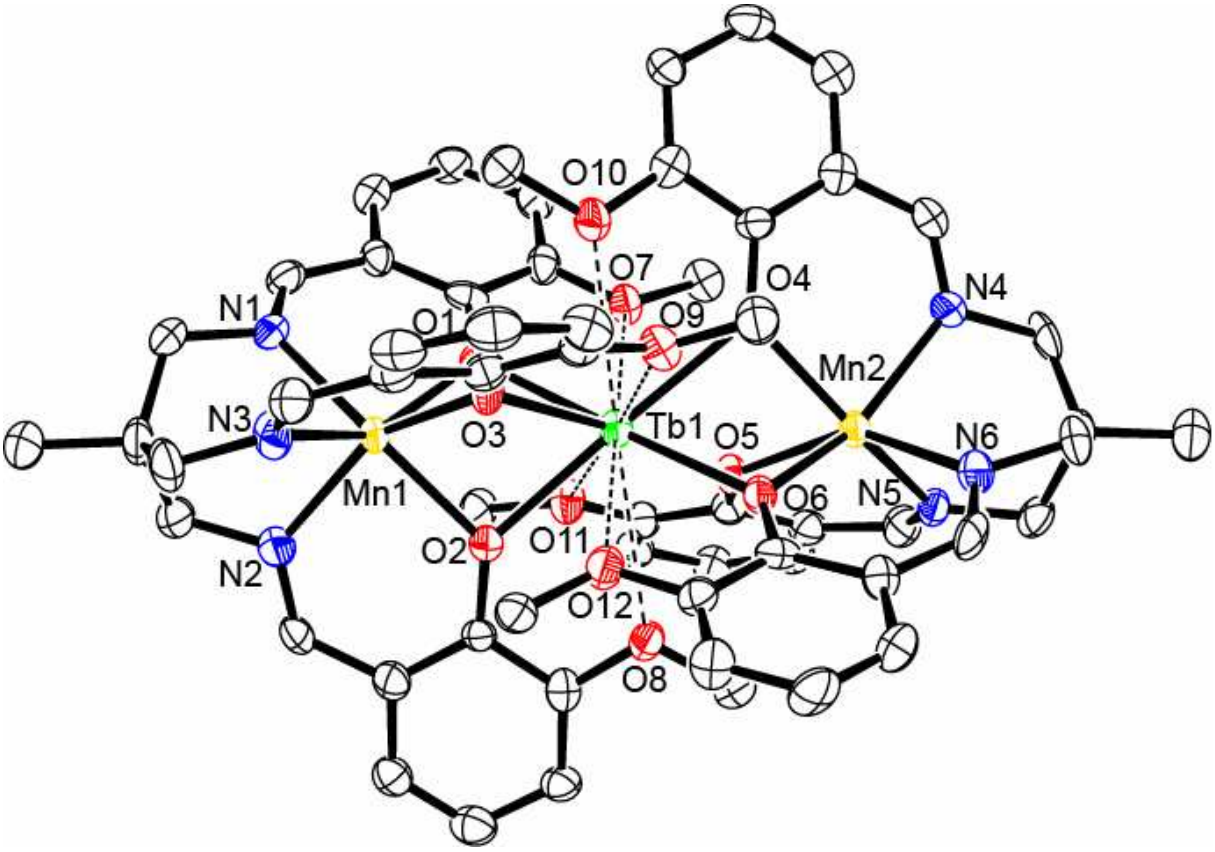

Figure S3. Molecular structure of the trinuclear $[LMnTbMnL]^{+}$ entity **6**, with the thermal ellipsoids drawn at the 30 % probability level. Hydrogen atoms are omitted for clarity.

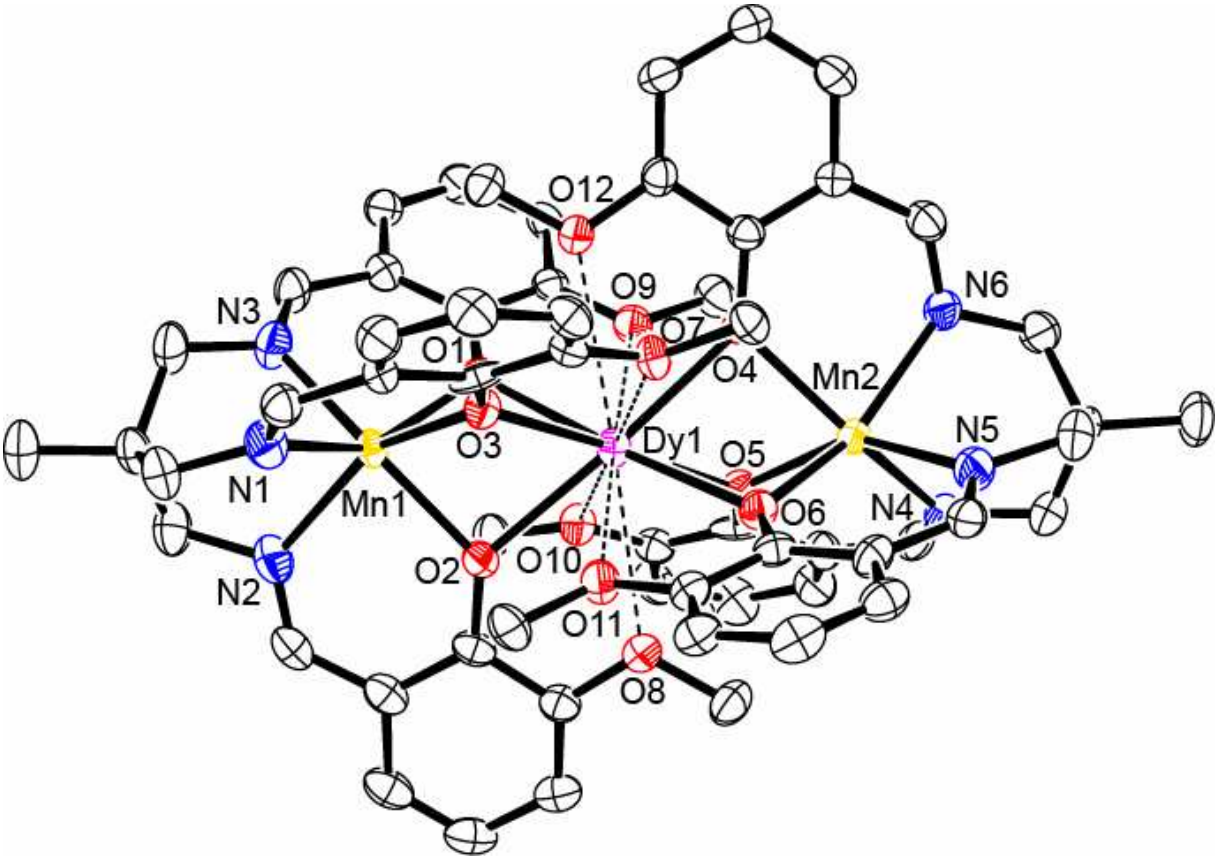

Figure S4. Molecular structure of the trinuclear $[LMnDyMnL]^{+}$ entity **7**, with the thermal ellipsoids drawn at the 30 % probability level. Hydrogen atoms are omitted for clarity.

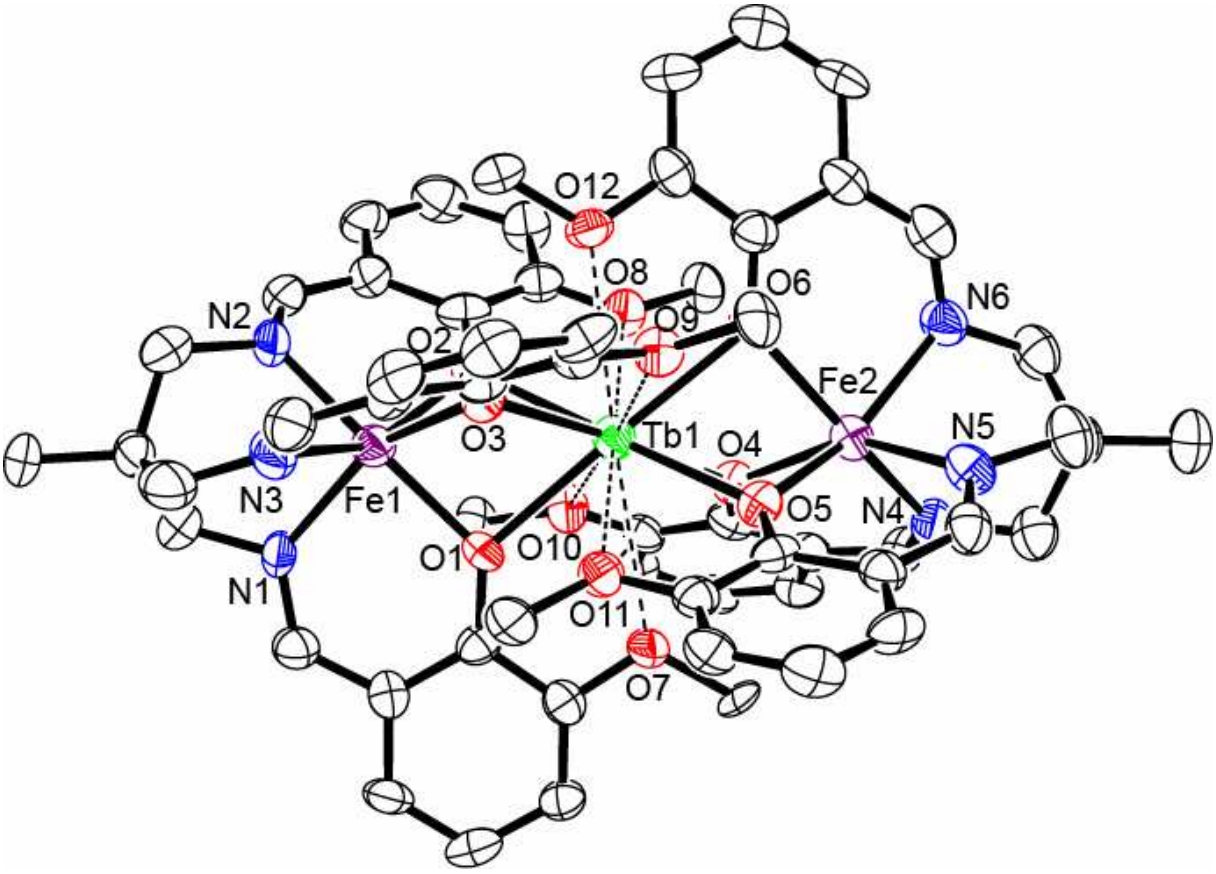

Figure S5. Molecular structure of the trinuclear $[LFeTbFeL]^{+}$ entity **9**, with the thermal ellipsoids drawn at the 30 % probability level. Hydrogen atoms are omitted for clarity.

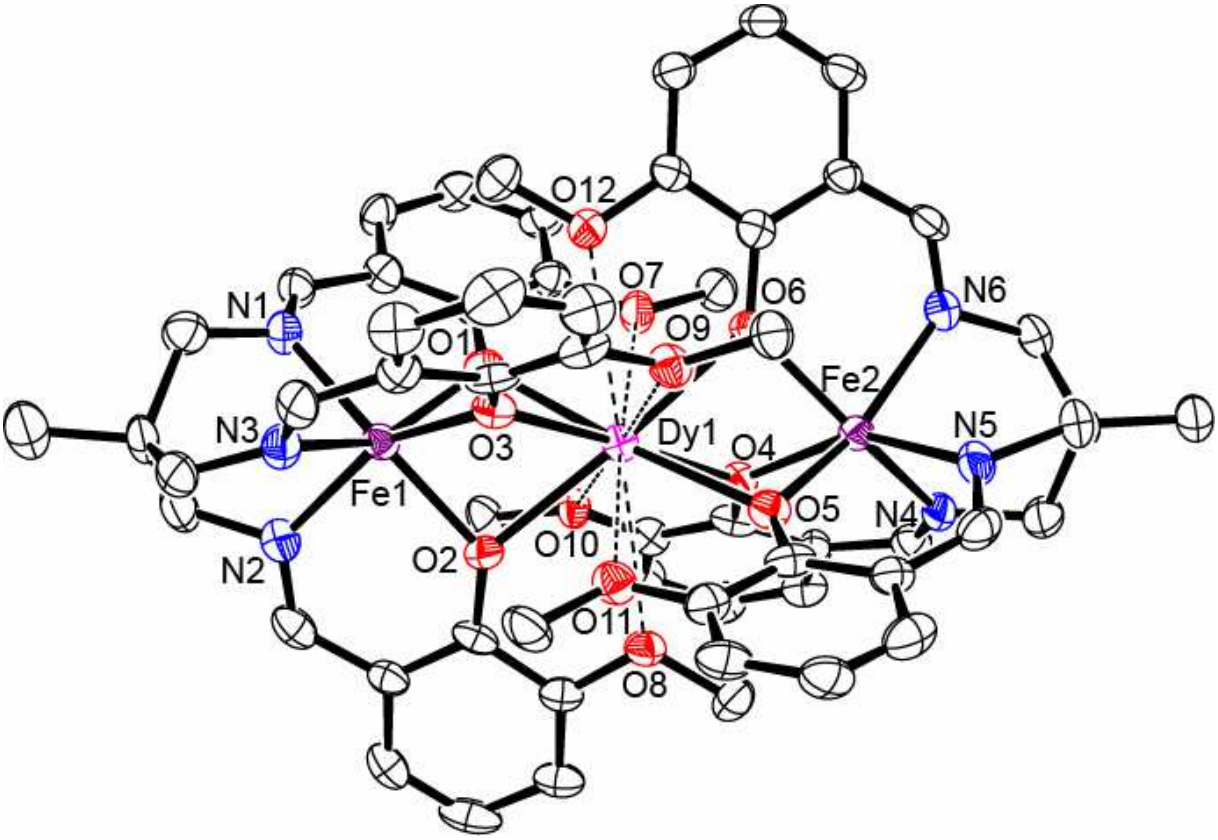

Figure S6. Molecular structure of the trinuclear $[LFeDyFeL]^+$ entity **10**, with the thermal ellipsoids drawn at the 30 % probability level. Hydrogen atoms are omitted for clarity.

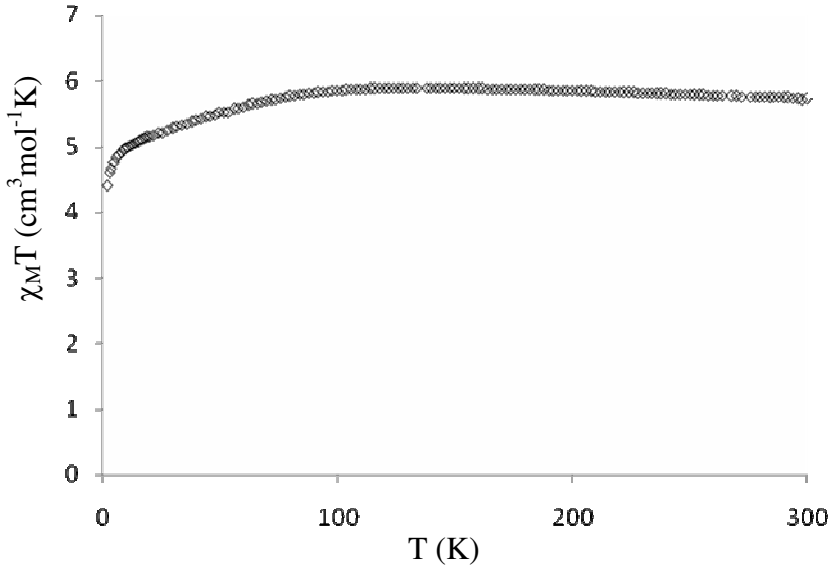

Figure S7. Temperature dependence of the $\chi_M T$ product for $[LCoLaCoL]NO_3 \cdot CH_3OH$ **4**.

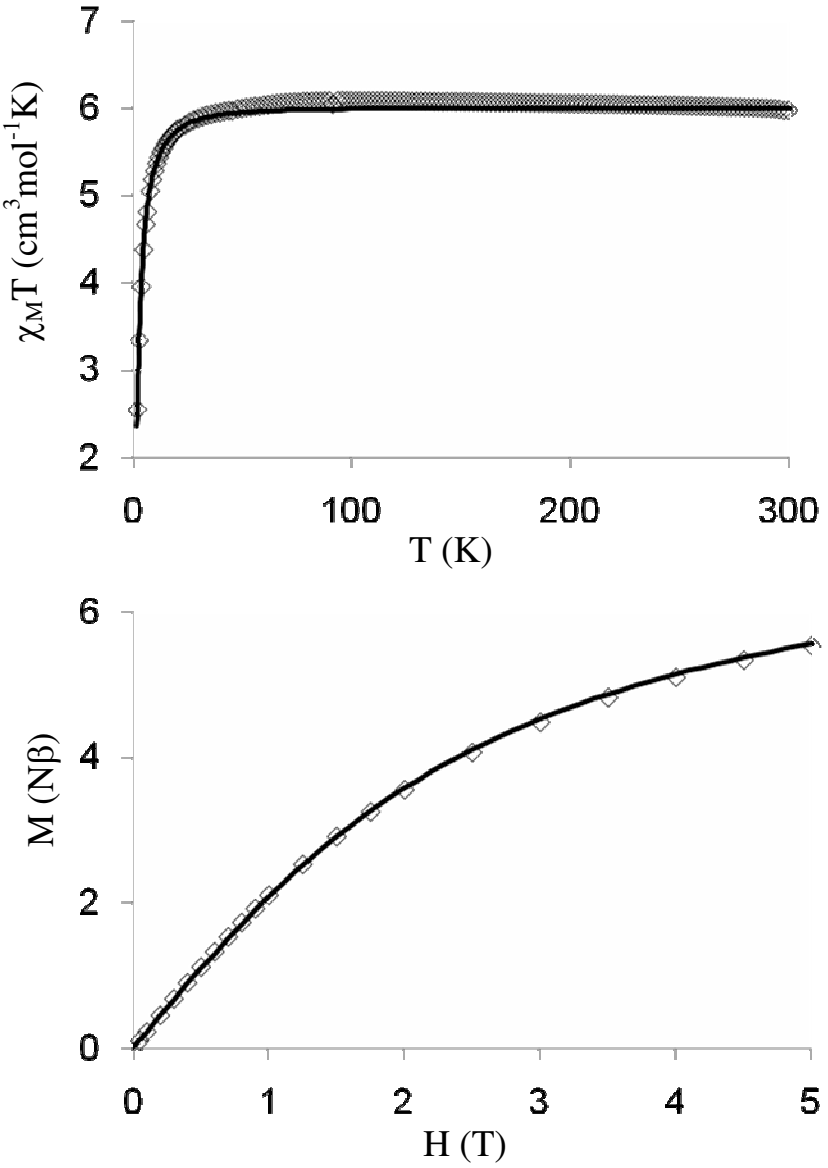

Figure S8. Temperature dependence of the product (top) and field dependence of the magnetization (bottom) for the [LFe-La-FeL]$ClO_4 \cdot CH_3OH$ complex **11**. The solid lines correspond to the best fits with D = 7 cm^{-1}, g = 2.0.

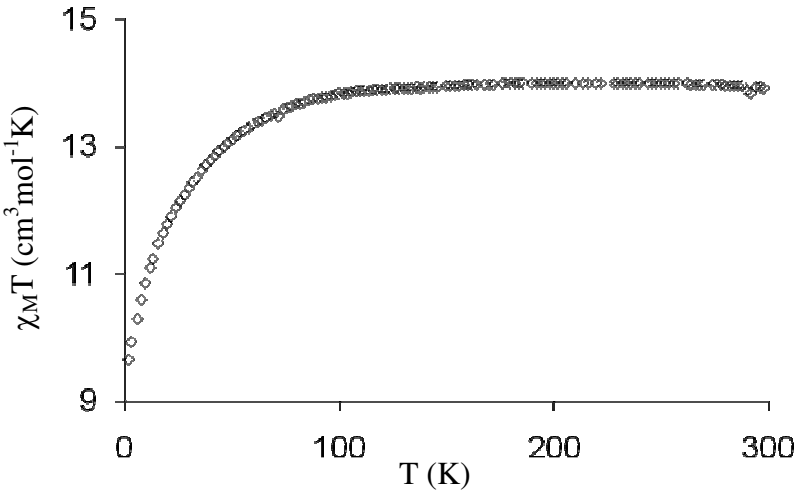

Figure S9. Temperature dependence of the $\chi_M T$ product for [LZnDyZnL]NO_3·2H_2O **13**.

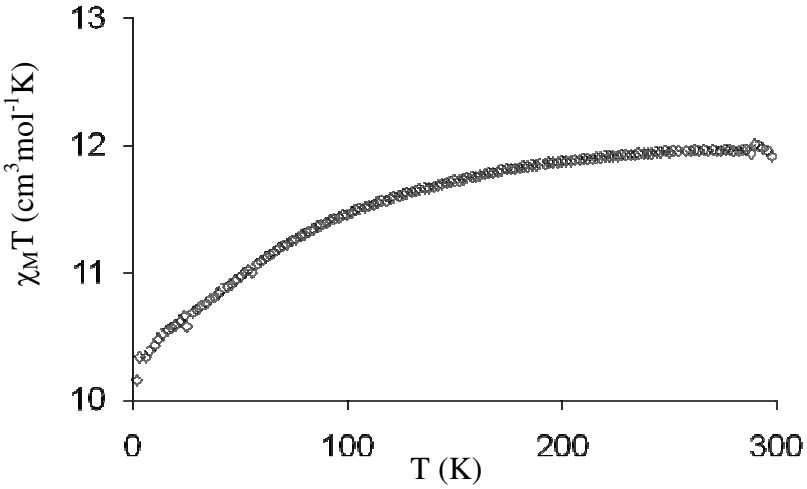

Figure S10. Temperature dependence of the $\chi_M T$ product for [LZnTbZnL]NO_3·3H_2O **12**.

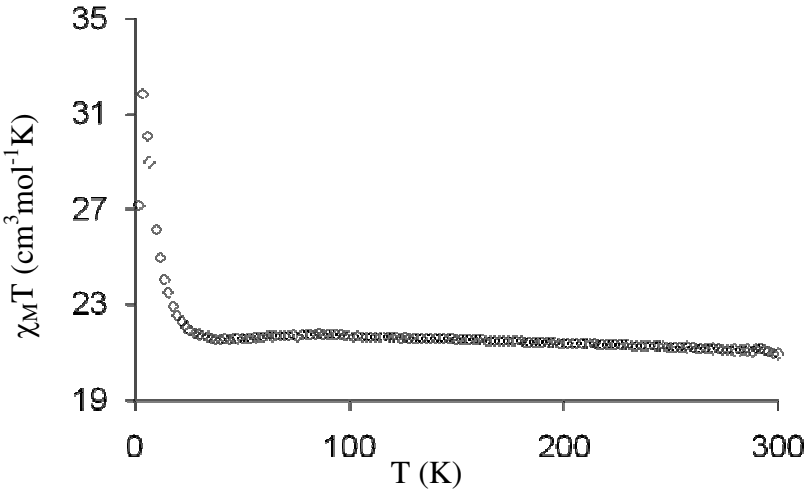

Figure S11. Temperature dependence of the $\chi_M T$ product for [LCoDyCoL]NO_3·CH_3OH **3**.

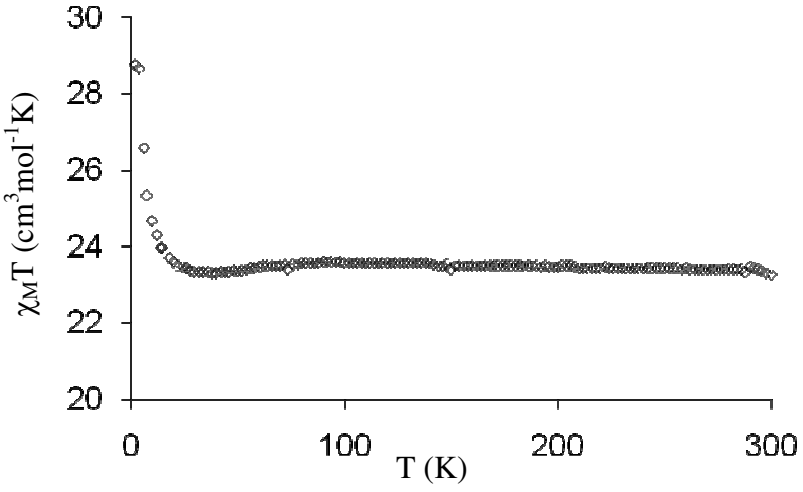

Figure S12. Temperature dependence of the $\chi_M T$ product for [LMnDyMnL]NO_3·CH_3OH **7**.

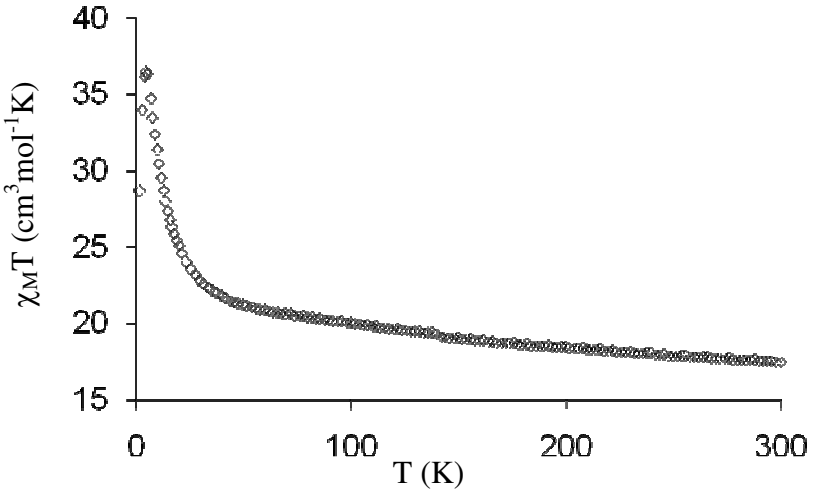

Figure S13. Temperature dependence of the $\chi_M T$ product for [LCoTbCoL]NO_3 **2**.

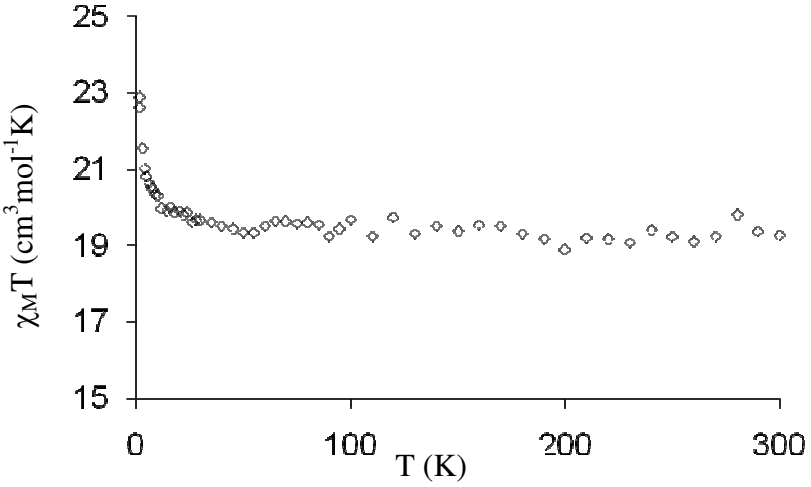

Figure S14. Temperature dependence of the $\chi_M T$ product for [LMnTbMnL]NO_3 **6**.

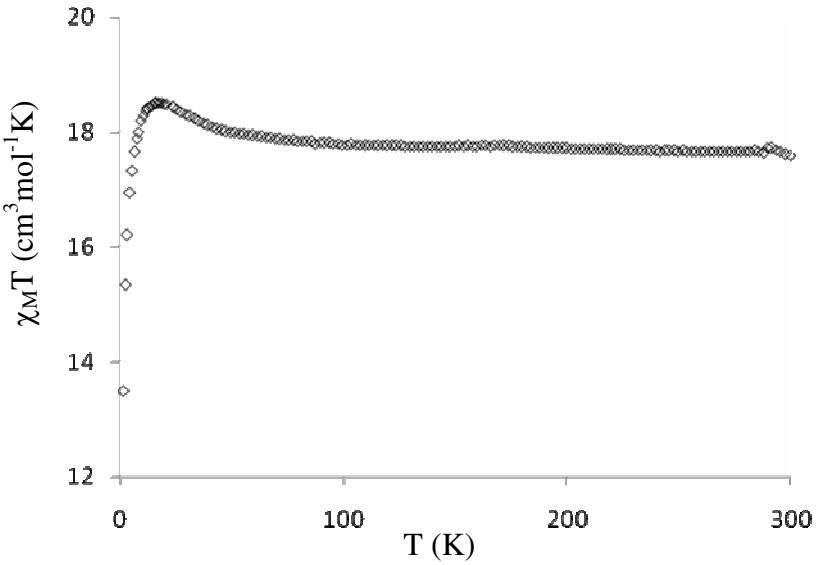

Figure S15. Temperature dependence of the $\chi_M T$ product for [LFeTbFeL]ClO_4·CH_3OH **9**.

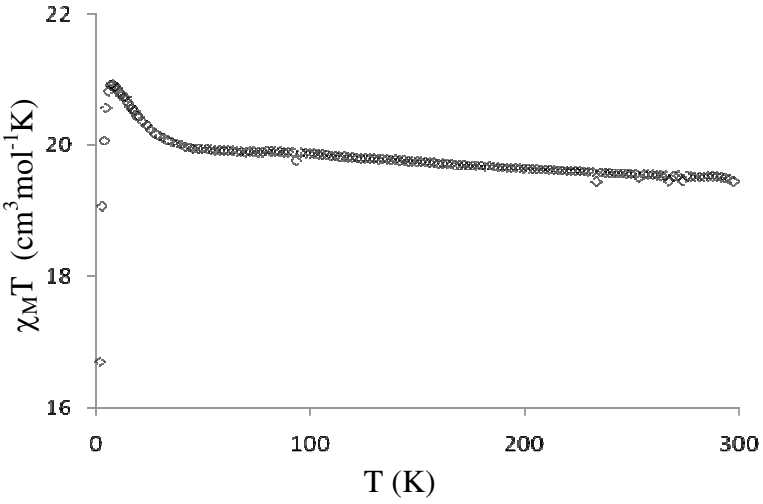

Figure S16. Temperature dependence of the $\chi_M T$ product for [LFeDyFeL]ClO_4·CH_3OH **10**.

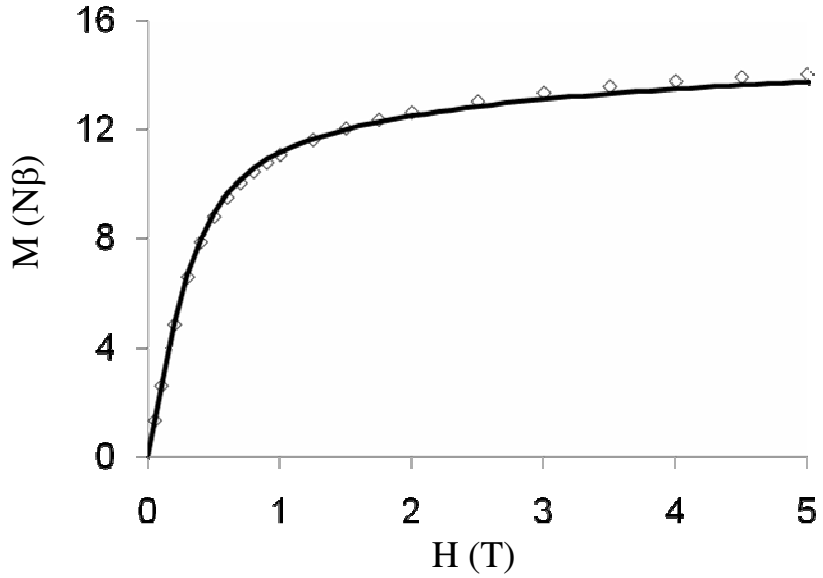

Figure S17. Field dependence of the magnetization for the [LFe-Gd-FeL]ClO_4 complex **8**. The solid line corresponds to the best fit with J = 0.69 cm^{-1}, D = 5.7 cm^{-1}, g = 2.04.

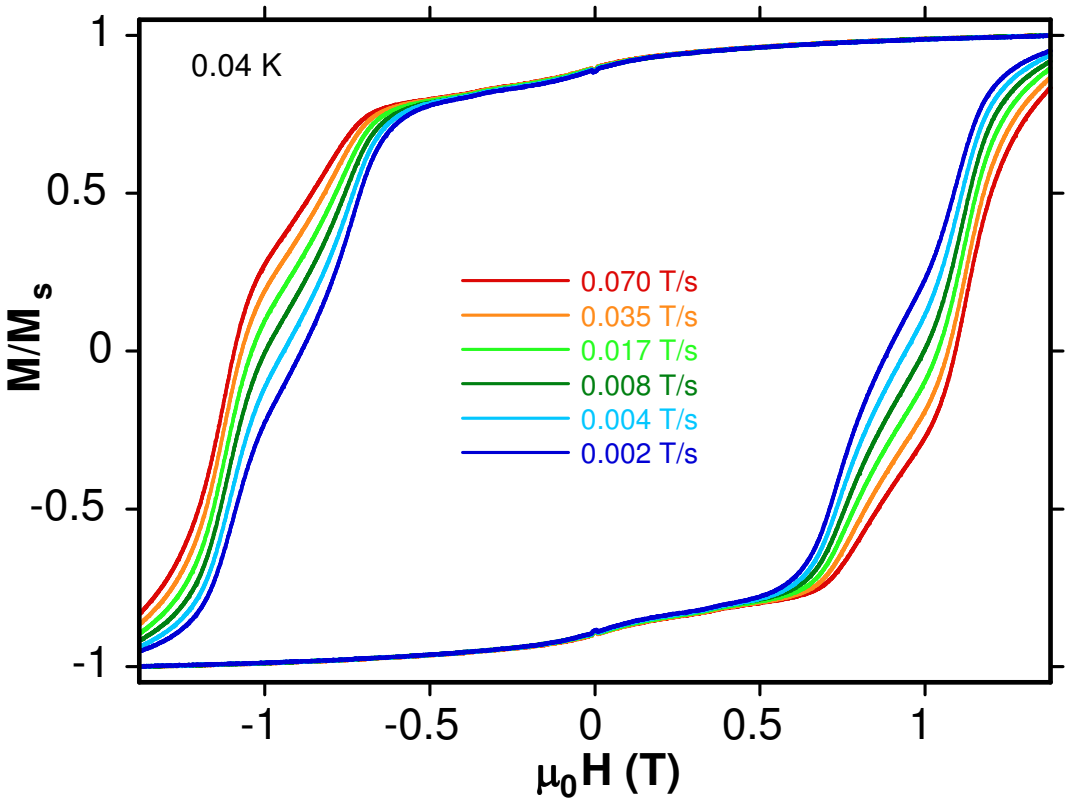

Figure S18. Magnetization M versus applied DC field H hysteresis loops for single crystals of **1** [LCoGdCoL]NO_3 at the indicated field sweep rates. The magnetization is normalized to its saturation value M_S at 1.4 T.

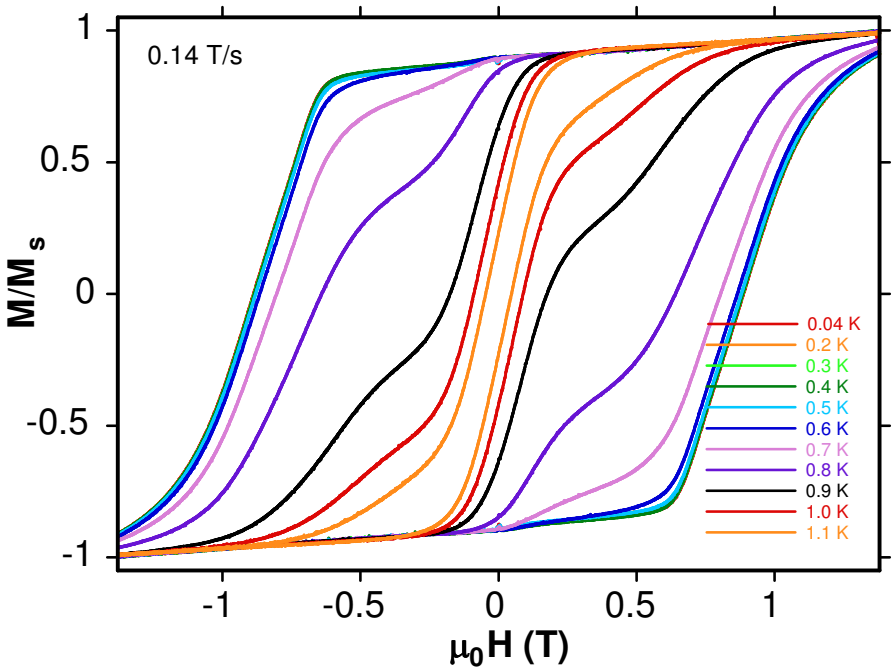

Figure S19. Magnetization M versus applied DC field H hysteresis loops for single crystals of **2** [LCoTbCoL]NO_3 at the indicated temperatures. The magnetization is normalized to its saturation value M_S at 1.4 T.

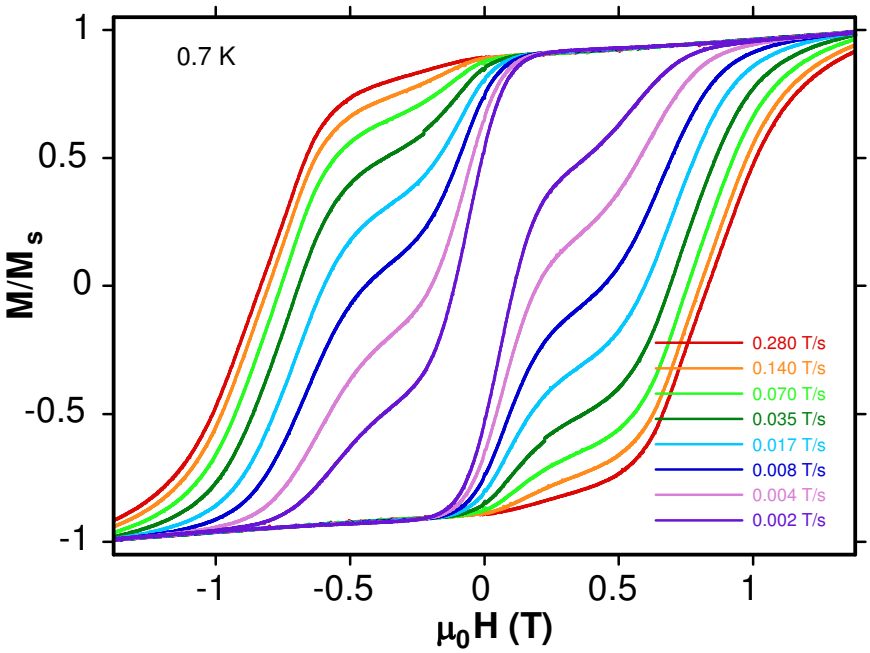

Figure S20. Magnetization M versus applied DC field H hysteresis loops for single crystals of **2** [LCoTbCoL]NO_3 at the indicated field sweep rates. The magnetization is normalized to its saturation value M_S at 1.4 T.

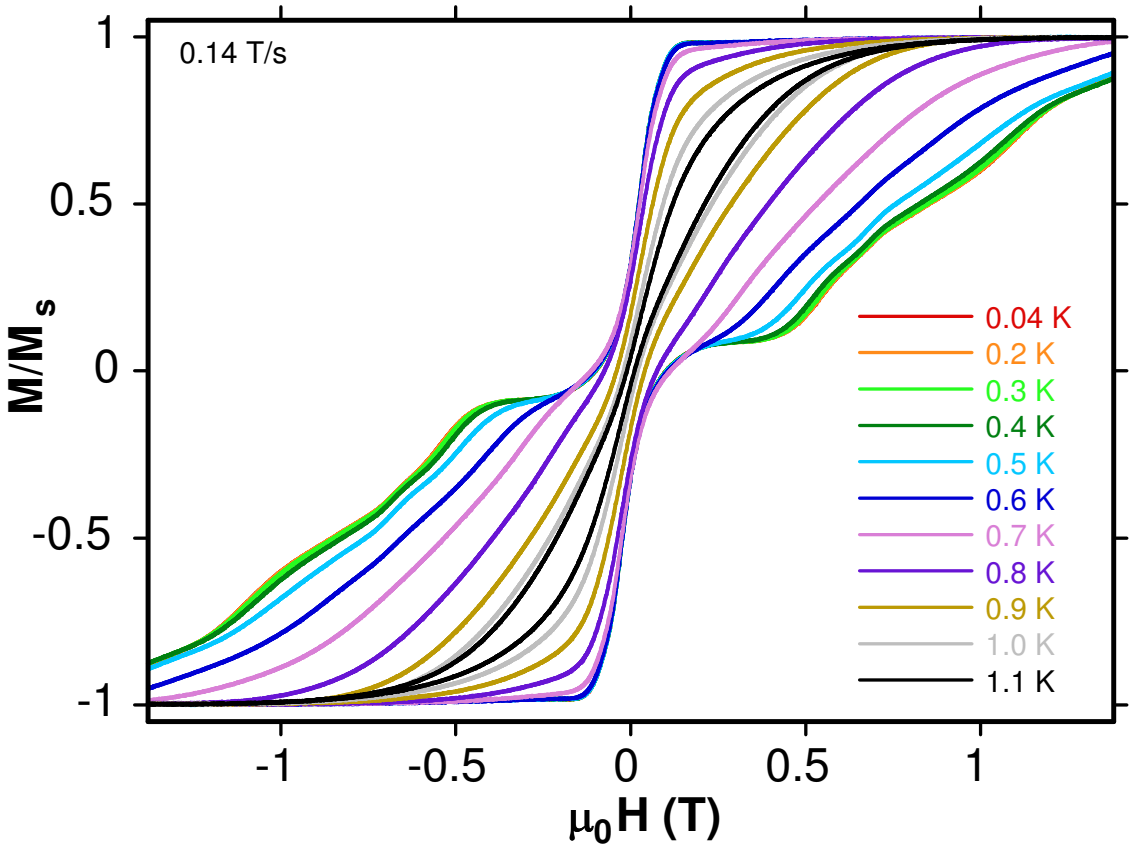

Figure S21. Magnetization M versus applied DC field H hysteresis loops for single crystals of **3** [LCoDyCoL]NO_3·CH_3OH at the indicated temperatures. The magnetization is normalized to its saturation value M_S at 1.4 T.

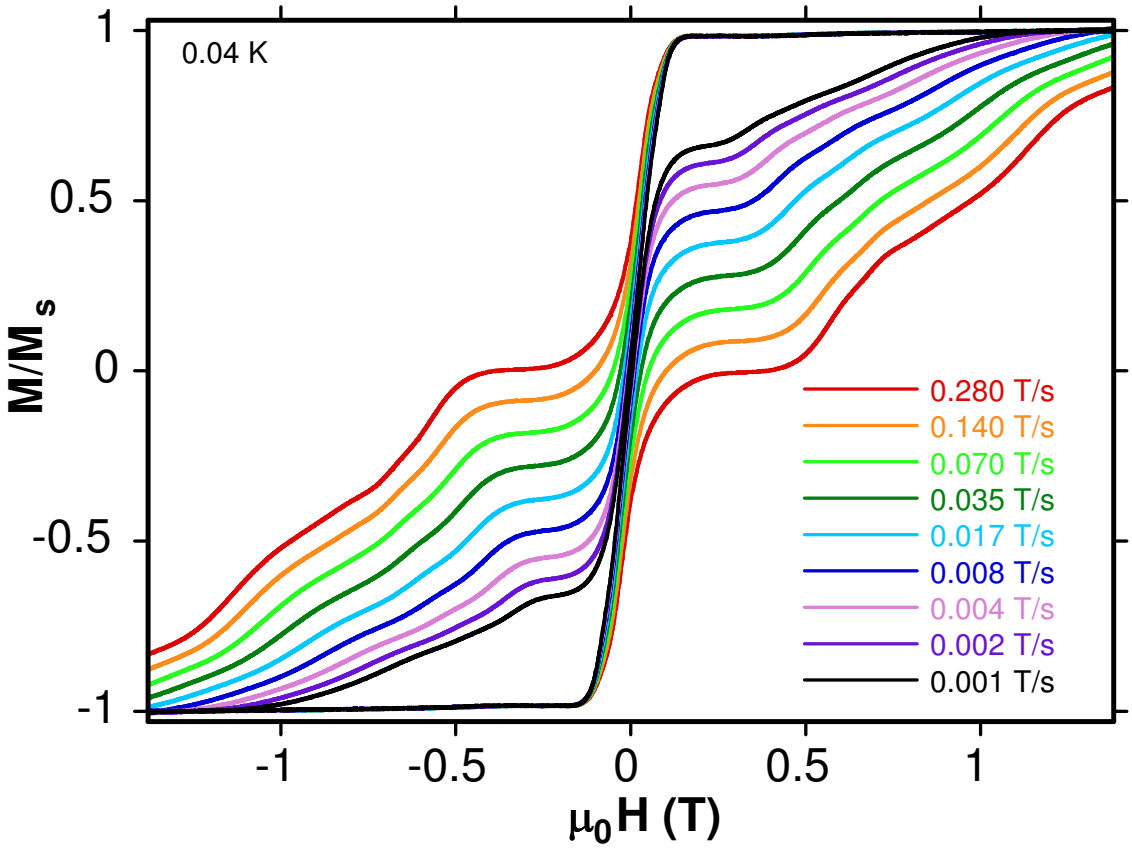

Figure S22. Magnetization M versus applied DC field H hysteresis loops for single crystals of **3** [LCoDyCoL]NO_3·CH_3OH at the indicated field sweep rates. The magnetization is normalized to its saturation value M_S at 1.4 T.

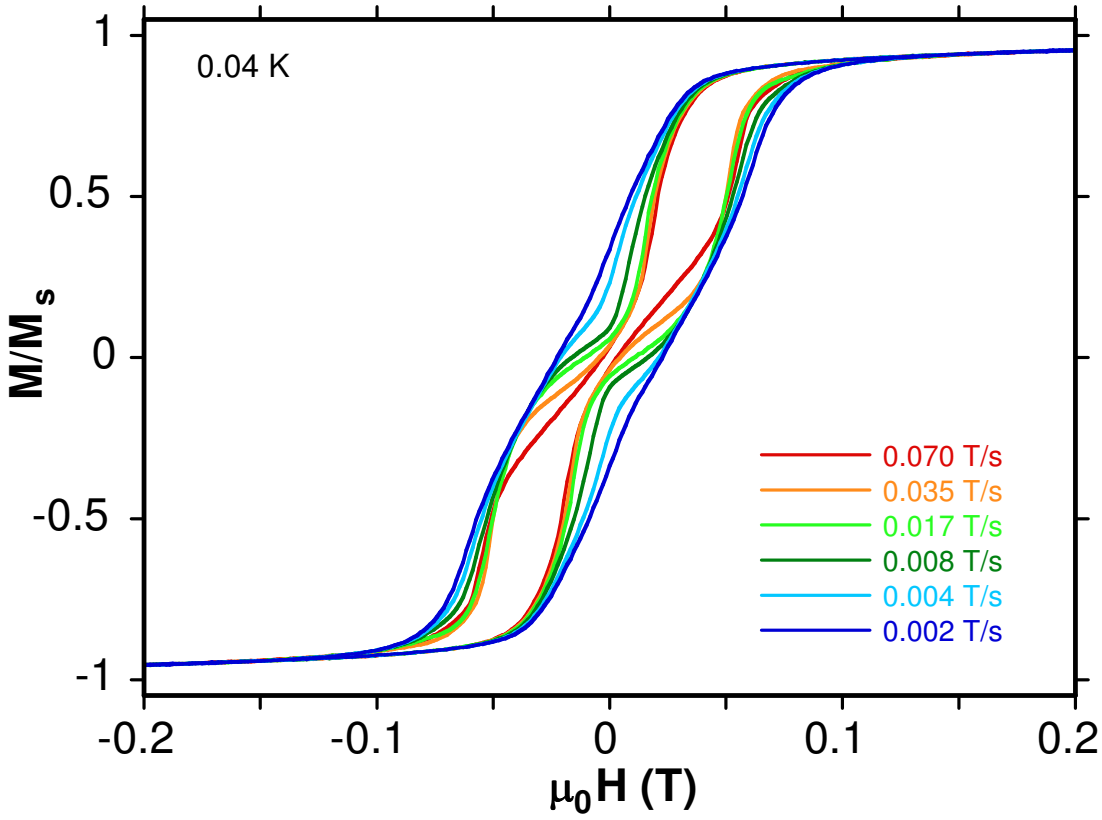

Figure S23. Magnetization M versus applied DC field H hysteresis loops for single crystals of **6** [LMnTbMnL]NO_3 at the indicated field sweep rates. The magnetization is normalized to its saturation value M_S at 1.4 T.

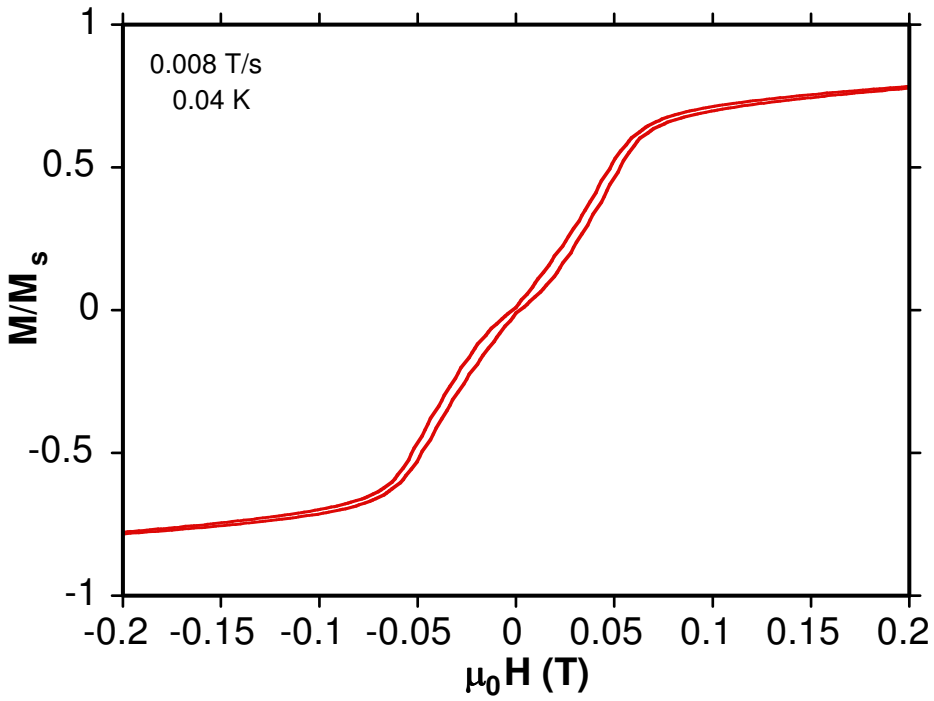

Figure S24. Magnetization M versus applied DC field H hysteresis loops for single crystals of **9** [LFeTbFeL]ClO_4·CH_3OH at 0.008 T/s field sweep rate and 0.04 K. The magnetization is normalized to its saturation value M_S at 1.4 T.

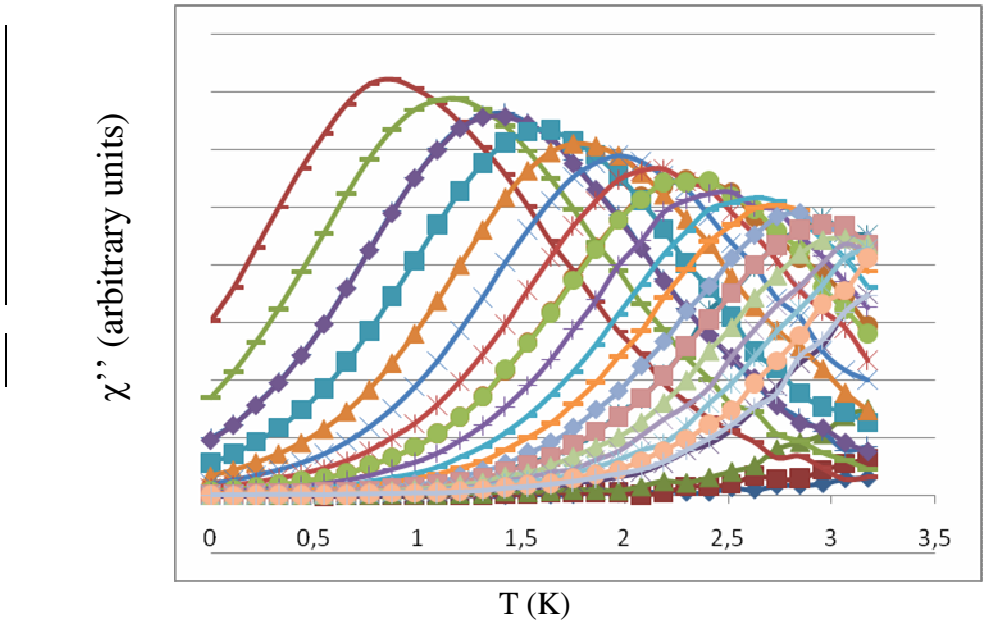

Figure S25. χ'' vs T data for ac frequencies ranging from 1 to 1500 Hz obtained at zero dc field on a polycrystalline sample of **1**.

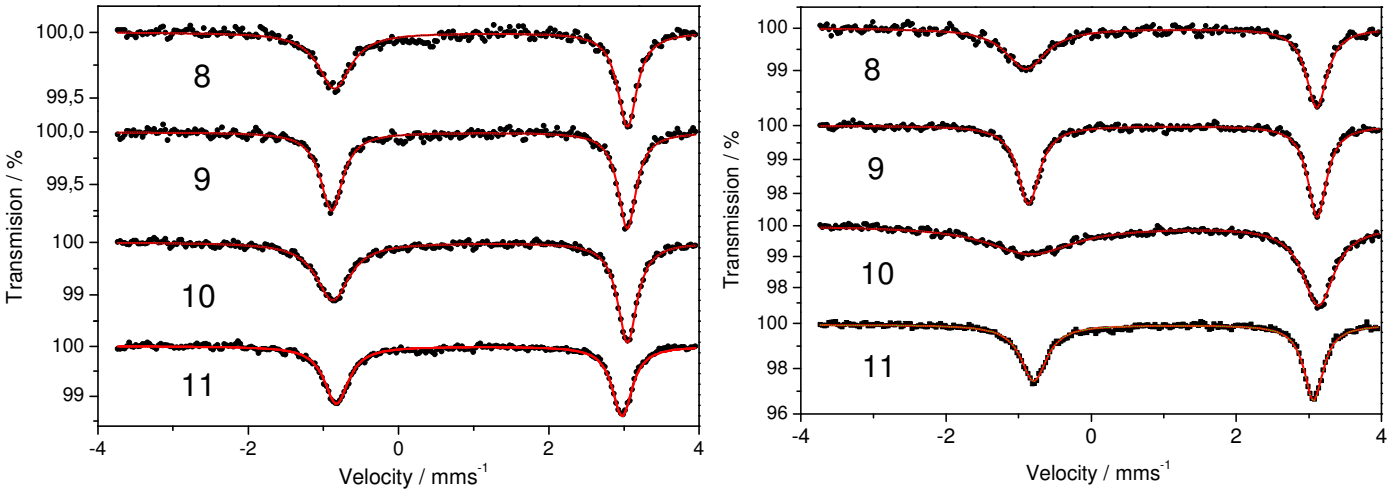

Figure S26. Mössbauer Parameters for Complexes [LFeGdFeL]ClO_4, **8**, [LFeTbFeL]$ClO_4 \cdot CH_3OH$, **9**, [LFeDyFeL]$ClO_4 \cdot CH_3OH$, **10**, and [LFeLaFeL]$ClO_4 \cdot CH_3OH$, **11**, at 200 (left) and 80 K (right).

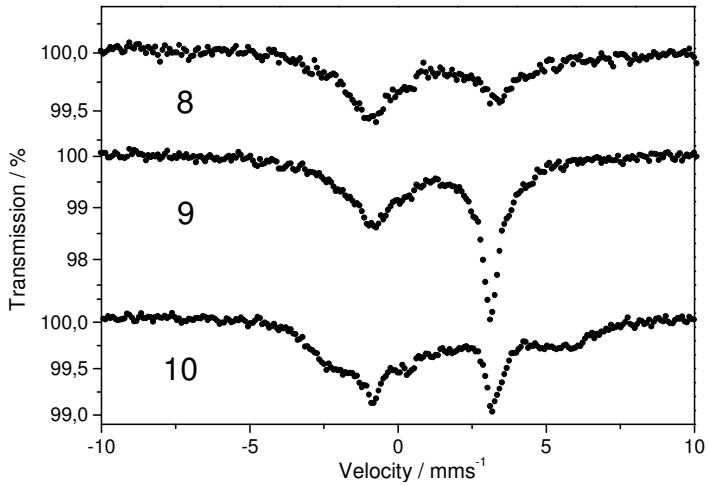

Figure S27. Mössbauer Parameters for Complexes [LFeGdFeL]ClO_4, **8**, [LFeTbFeL]$ClO_4 \cdot CH_3OH$, **9** and [LFeDyFeL]$ClO_4 \cdot CH_3OH$, **10**, at 5 K.